ACS OMEGA

http://pubs.acs.org/journal/acsodf

Article

Bolt−Cable−Mesh Integrated Support Technology for Water Drenching Roadway in Thick Coal Seam

Ce Jia, Sheng Li,* Chaojun Fan, Mingkun Luo, Lijun Zhou, Ziang Pu, and Lei Yang

Cite This: *ACS Omega* 2022, 7, 46682−46692

Read Online

ACCESS | Metrics & More | Article Recommendations

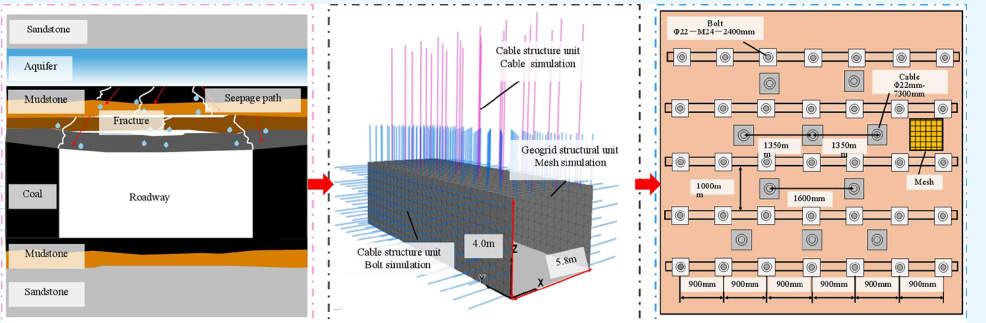

Water - rock interaction of thick coal seam in water-drenching roadway

Numerical model of surrounding rock support in 2606 roadway

Effect drawing of on-site support of 2606 transport roadway

ABSTRACT: Aiming at the problems of large deformation and difficult control of the mining roadway water drenching in a thick coal seam, the principle of double-arch zoning cooperative surrounding rock control is studied by using the combined method of theoretical analysis, numerical simulation, and industrial experiment. The water−rock interaction of the surrounding rock of water-drenching roadway is proposed, taking into account the damage to the mechanical parameters of the surrounding rock caused by soaking water. The water-mechanical-damage coupling model for surrounding rock of a coal seam roadway is constructed, and is numerically solved by the code development using the FISH language. The principle of "high prestressed bolt−cable−mesh" zone coordinated control is revealed, and the existence of a compressive stress arch is verified by FLAC^{3D} software. The three support schemes were compared and analyzed by numerical simulation software. We affirmed the bolt length of 2400 mm, spacing of 0.9 m, row spacing of 1 m, cable length of 7300 mm, and arrangement 3−2−3 as the optimal support scheme and applied this scheme in the Zhangcun Coal Mine. The results show that the maximum deformation of the roadway roof is 142 mm, and the ultimate convergence of the two sides is 83 mm. The surrounding rock has been effectively controlled.

1. INTRODUCTION

China's coal mines are mainly underground, with 12,000 km of newly excavated roadways yearly.[1,2] According to incomplete statistics, more than 80% of the roadways are coal roadways.[3,4] The number of deaths caused by coal mine roof accidents accounts for 33.8% of all accident deaths in coal mines.[5,6] Effectively controlling the surrounding rock is necessary to guarantee the safe and high production of the mine.[7] Coal mining encounters complex geological environments. Therefore, roadway-surrounding rock support in complex and challenging conditions is one of the urgent problems in the process of coal safety production.[8,9] When the roadway is in a water-drenching environment, the mechanical parameters of the surrounding rock will be weakened under the action of water leaching for a long time.[10,11] The large deformation of the surrounding rock makes support extremely difficult.[12] It increases the maintenance cost and volume of the roadway, which seriously hinders the safe and efficient production of the mine.[13,14]

At present, scholars at home and abroad have researched and explored the problems of large deformation and complex control of roadways under water-drenching conditions. The research mainly includes simulating the damage mechanism of a high-stress soft-rock roadway under drenching conditions with FLAC3D software,[15] simulating the mechanical properties of a water-rich soft-rock roadway from the perspective of fluid−solid coupling with GTS software,[16] and simulating and analyzing the damage characteristics of surrounding rock under different section conditions of water-rich roadway.[17] FLAC^{3D} software utilizes the finite difference method compared to

Received: September 1, 2022
Accepted: November 21, 2022
Published: December 8, 2022

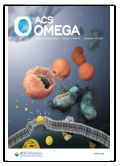

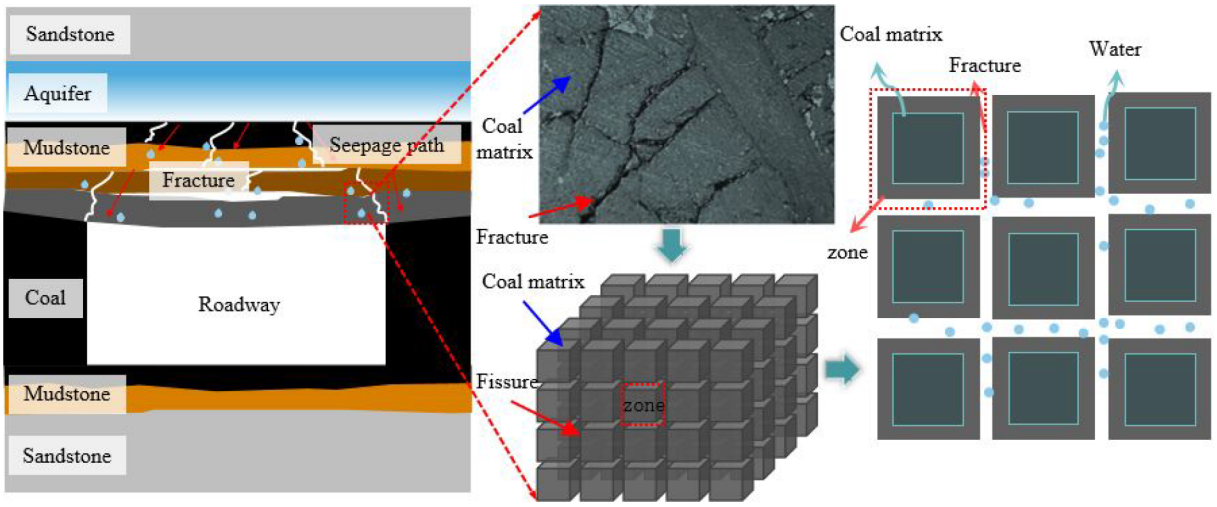

Figure 1. Water−rock interaction of thick coal seam in water-drenching roadway.

other numerical simulation software. The software can effectively solve significant deformation problems, and deformation discontinuity is suitable for geotechnical deformation research. Kang[18] believed that the drenching roadway surrounding rock has explicit mechanical properties of soft rock. Małkowski[19] simulated the drenching roadway using the finite element phase 2 program and obtained that the strength and strain parameters of the rock gradually decrease with increasing water content leading to increased deformation of the surrounding rock. It is shown that the mechanical properties of the rock surrounding the drenching tunnel are similar to those of soft rock. Scholars at home and abroad have done a lot of exploratory work on soft-rock and drenching roadway support.[20−22] For example, He[23] proposed to control the stability of a composite soft-rock roadway with constant resistance large deformation mesh cable coupling support technology. Tan[24] proposed a cooperative deformation mechanism between bolts and surrounding rock under high pressure to control weakly cemented soft-rock roadways. Zhang[25] proposed a multilayered coupled support method of bolts and ring braces to achieve deep high-stress soft-rock roadway-surrounding rock control. Yang[26] investigated the mechanism and control method of laminar floor instability in soft-rock roadways using a combination of numerical simulation and mechanical analysis. Cai[27] proposed a high-strength and high-prestress "inverted trapezoid" cable−mesh−beam support structure + straight wall cut arch roadway section + full-section shotcrete coupled surrounding rock control method. However, the above research only considers the effect of the seepage field on support. The impact of the combined effect of groundwater weakened coal rock mechanical parameters, and the seepage pressure field on the support was not considered.[28] In addition, the control methods and measures of the surrounding rock in water-drenching roadway in thick coal seams have not been researched.

In this paper, we consider the effects of groundwater on the mechanical damage of coal rock mass and the impact of pore pressure on the effective stress, and build a coupled water-mechanical-damage mathematical model. The secondary development of the FLAC^{3D} software is performed through the FISH language, and the coupled model is solved numerically. The principle of "high prestressed bolt, cable + mesh" zoning cooperative control is revealed. The distribution law of stress, displacement, and plastic zone of the roadway surrounding rock under three support schemes is comparatively studied. The optimal solution and parameters were obtained by numerical simulation, and relevant on-site industrial tests were carried out.

2. MATHEMATICAL MODEL OF WATER-MECHANICAL-DAMAGE COUPLING IN SURROUNDING ROCK OF THICK COAL SEAM WATER-DRENCHING ROADWAY

2.1. Basic Assumptions of the Model. The deformation of the roadway surrounding rock under groundwater seepage pressure leads to changes in the pore/fissure structure and space in the surrounding rock, which affects the distribution of the groundwater seepage field, as shown in Figure 1. The following assumptions are based on the characteristics of groundwater flowing in the surrounding rock: (1) The coal rock mass is a porous medium. The equivalent continuous medium model can simulate the porous continuous medium's surrounding rock. (2) The flow of groundwater in the surrounding rock satisfies Darcy's law and Biot's equation.[29,30] (3) The coupling of groundwater seepage, stress, and damage fields will lead to the deformation and damage of the roadway surrounding rock. The water-mechanical-damage coupled mathematical model of the roadway surrounding rock mainly includes controlling equations such as equilibrium, motion, constitutive, and continuity.

2.2. Governing Equations of the Water-Mechanical-Damage Coupling Model.

(1) Groundwater seepage field equation.

The mass balance equation of groundwater seepage is[31]

$$-q_{i,i} + q_v = \frac{\partial \zeta}{\partial t} \tag{1}$$

where q_i is the seepage velocity, m/s; q_v is the fluid source strength, L/s; ζ is the change in fluid volume per unit volume of coal and rock.

Groundwater seepage conforms to Dacry's law, assuming that coal and rock are homogeneous and isotropic materials, the equation is expressed as follows:[32]

$$q_i = -k[p - \rho_f x_j g_j]_{,i} \tag{2}$$

https://doi.org/10.1021/acsomega.2c05650
ACS Omega 2022, 7, 46682−46692

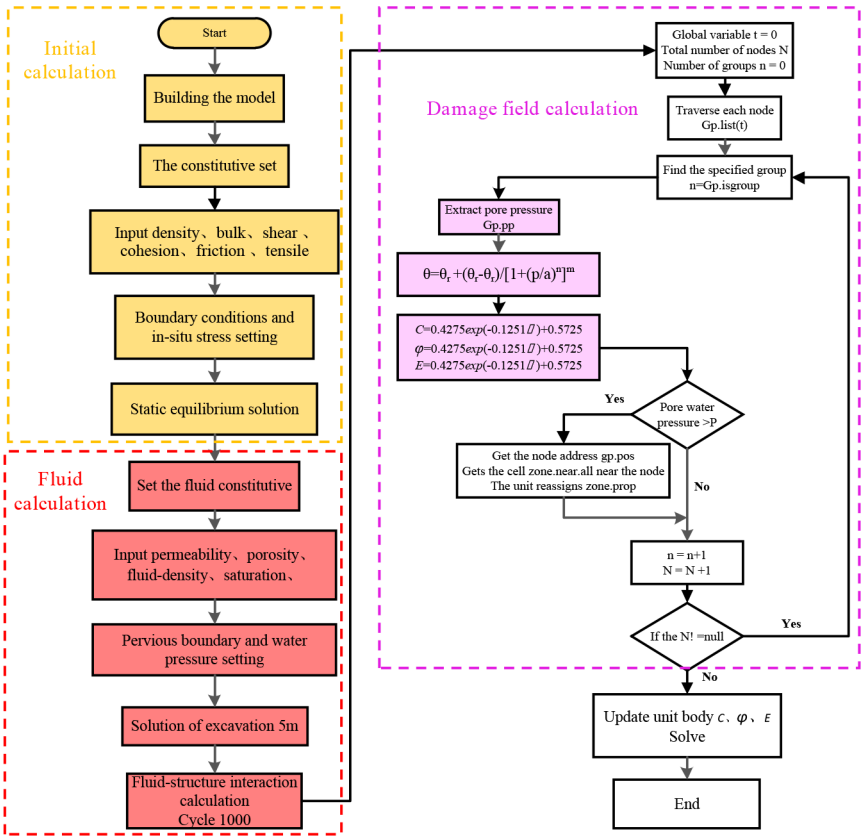

Figure 2. Water-mechanical-damage coupling development flowchart.

where q_i is the seepage velocity, m/s; k is the permeability coefficient of the medium, m^2/Pa s; ρ_w is the fluid density, kg/m^3; x_j is the velocity component of the medium, m/s; g_j is the gravitational acceleration component, m/s^2.

Assuming that the surrounding rock is a porous medium, the seepage constitutive equation of the surrounding rock is[33]

$$\frac{1}{M}\frac{\partial p}{\partial t} + \frac{n}{s}\frac{\partial s}{\partial t} = \frac{1}{s}\frac{\partial \zeta}{\partial t} - \alpha\frac{\partial \varepsilon}{\partial t} \tag{3}$$

where M is the Biot modulus, N/m^2; p is the pore pressure, Pa; α is the Biot coefficient; ε is the strain induced by the stress field; s is the saturation; n is the porosity.

Substitute eq 1 into eq 3 to obtain the continuity equation of groundwater seepage:

$$\frac{1}{M}\frac{\partial p}{\partial t} + \frac{n}{s}\frac{\partial s}{\partial t} = \frac{1}{s}(-q_{i,i} + q_v) - \alpha\frac{\partial \varepsilon}{\partial t} \tag{4}$$

(2) Stress field coupling equation.

When the effective stress in the coal rock medium changes, the volumetric strain also changes, resulting in a change in the pore pressure within the fluid. On the contrary, the volume strain also changes if the pore pressure changes. The incremental basic form of the pore medium constitutive equation is

$$\Delta\overline{\sigma_{ij}} + \alpha\Delta p\delta_{ij} = H_{ij}(\sigma_{ij}, \Delta\xi_{ij}) \tag{5}$$

where $\Delta\overline{\sigma_{ij}}$ is the effective stress increment; Δp is the pore pressure increment; ξ_{ij} is the Kronecher constant; H_{ij} is a given function; $\Delta\xi_{ij}$ is the total strain increment.

(3) Damage field equation.

When the surrounding rock is in the soaking water environment, the groundwater will have physical, chemical, and mechanical effects on the surrounding rock. The mudstone encounters water, mudding, disintegration, expansion, and fragmentation will occur, and the mechanical properties will be weakened, leading to large deformation of the surrounding rock. The number of fractures in the surrounding rock increases under groundwater infiltration, thereby providing more transmission channels for water migration to produce seepage phenomena. Pore pressure can cause a change in effective stress, which significantly changes the fracture opening. When the surrounding rock is soaked, the strength decreases significantly, and this effect becomes more evident with increased time.[30] Therefore, the mechanics of the roadway surrounding rock depends on the water content of the roadway surrounding rock. There is a functional relationship between pore pressure and water content, and the pore pressure can be used to invert the water content of the surrounding rock. The functional equation of pore water pressure and water content is proposed in the literature:[34,35]

$$\theta = \theta_r + \frac{\theta_s - \theta_r}{[1 + (p/a)^n]^m} \tag{6}$$

where θ is the volumetric moisture content; θ_r is the residual volumetric moisture content; θ_s is the saturated volumetric moisture content; p is the pore pressure, pa; m takes the value 1, and n takes the value 10.

Groundwater seepage mainly affects cohesion, internal friction angle, and elastic modulus in the mechanical parameters of surrounding rock. According to the mine geological data, the anchor end is located in the mudstone.

https://doi.org/10.1021/acsomega.2c05650
ACS Omega 2022, 7, 46682−46692

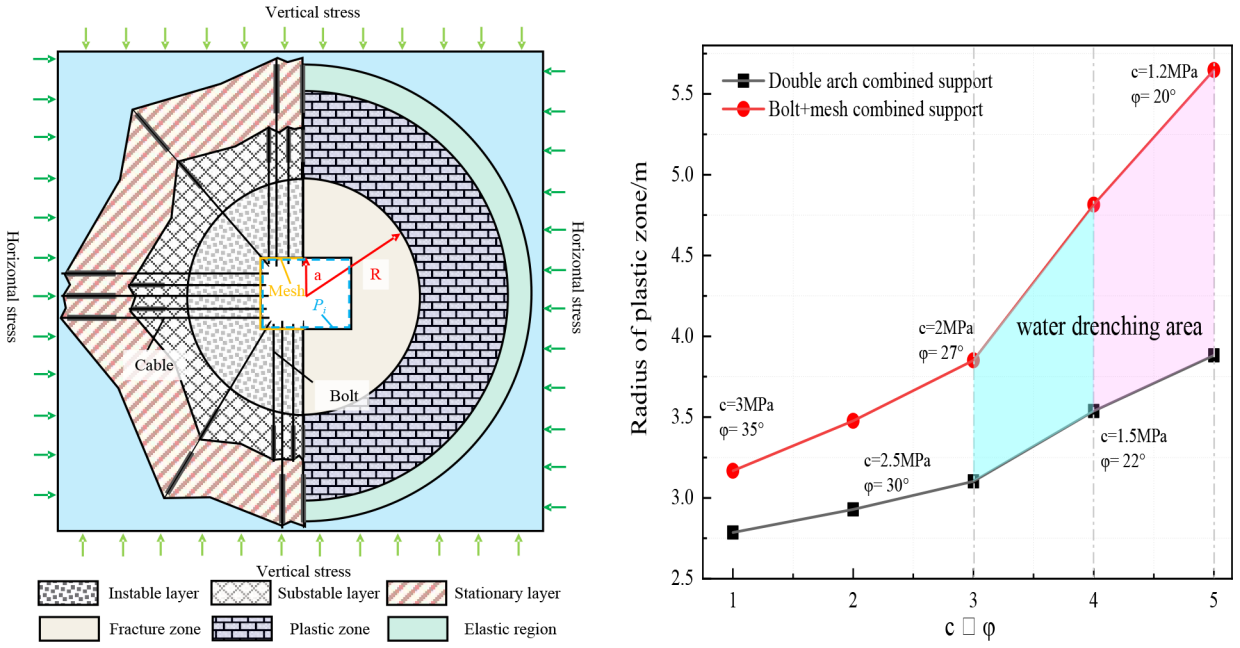

Figure 3. Double arch cooperative partition control model of surrounding rock.

When the mudstone encounters water, the mudstone will soften and swell to reduce the anchoring effect. Therefore, combined with previous research, this paper introduces the water softening coefficient to describe the water softening of surrounding rock.[36−42]

$$\begin{cases} c = 0.4275\exp(-0.125\eta) + 0.57 \\ \varphi = 0.0399\exp(-0.169\eta) + 0.96 \\ E = 0.5709\exp(-0.133\eta) + 0.42 \end{cases} \quad (7)$$

where c is the cohesive force softening coefficient; φ is the internal friction angle softening coefficient; E is the elastic modulus weakening coefficient; η is the water content.

2.3. Numerical Realization of Water-Mechanical-Damage Coupling Model Based on FLAC^{3D} Software. The mathematical model constructed according to section 2.2 is solved in FLAC^{3D} software. Based on the control equation of the water-mechanical-damage coupling model, a new flow-solid coupling method is defined using the FISH language to realize the softening of the roof of the drenching roadway, as shown in Figure 2. The main implementation steps for performing the solution in the software are as follows:

Step 1: First, the mechanical calculation of the model is performed. Build the model, set the intrinsic and boundary conditions. Restore the ground stress environment for hydrostatic solution.

Step 2: Set up fluid instants, fluid parameters, and permeability boundary. The tunnel is excavated 5 m, and 1000 steps are calculated to simulate the surrounding rock stress release and groundwater seepage.

Step 3: Import the self-designed FISH damage field equation, traverse each model node and find the specified grouping. Extraction of pore pressures for the developed subgroups. The water content is calculated according to eq 6. The values of c, φ, and E at different water contents are obtained according to eq 7. Built-in commands update the mechanical parameters of the surrounding rock (gp.pos, zone.near.all, zone. prop), and the process is shown in Figure 2.

Step 4: In opening the seepage calculation, mechanical calculation, and solving the equilibrium.

3. SURROUNDING ROCK CONTROL PRINCIPLE OF WATER-DRENCHING ROADWAY IN THICK COAL SEAM

Due to the different load-bearing capacities of each zone of the surrounding rock, the surrounding rock was divided into unstable, nonstable, and stable layers from inside to outside.[43] After excavating the roadway, the surrounding rock is divided into a fracture, plastic, and elastic zone from inside to outside. The plastic zone is the primary load-bearing zone of the surrounding rock, and once large deformation occurs, the self-bearing capacity of the surrounding rock decreases. Therefore, the size of the radius R of the plastic zone is an essential factor in determining the stability of the surrounding rock.

Based on the elastic-plastic mechanics, the radius R of the plastic zone of the roadway is derived.[44]

$$R = a\left[\frac{(p_0 + c\cot\varphi)(1-\sin\varphi)}{P_i + c\cot\varphi}\right]^{1-\sin\varphi/2\sin\varphi} \quad (8)$$

where R is the radius of the plastic zone, m; P_0 is the initial primary rock stress, MPa; P_i is the support resistance, MPa; φ is the angle of friction, deg; c is internal cohesion, MPa; $a = K\sqrt{\frac{S}{\pi}}$, the rectangular section roadway K takes 1.2;[45] S is the cross-sectional area of the roadway, m^2.

To effectively reduce the local stress concentration in the surrounding rock and avoid considerable area plastic damage, the double-arch zoning control method of "high prestressed bolt, cable + mesh" is adopted, as shown in Figure 3a. According to the literature,[46] the support resistance of the support structure is related to its own parameters and arrangement method. The bolt support resistance is P_b as follows:

https://doi.org/10.1021/acsomega.2c05650
ACS Omega 2022, 7, 46682−46692

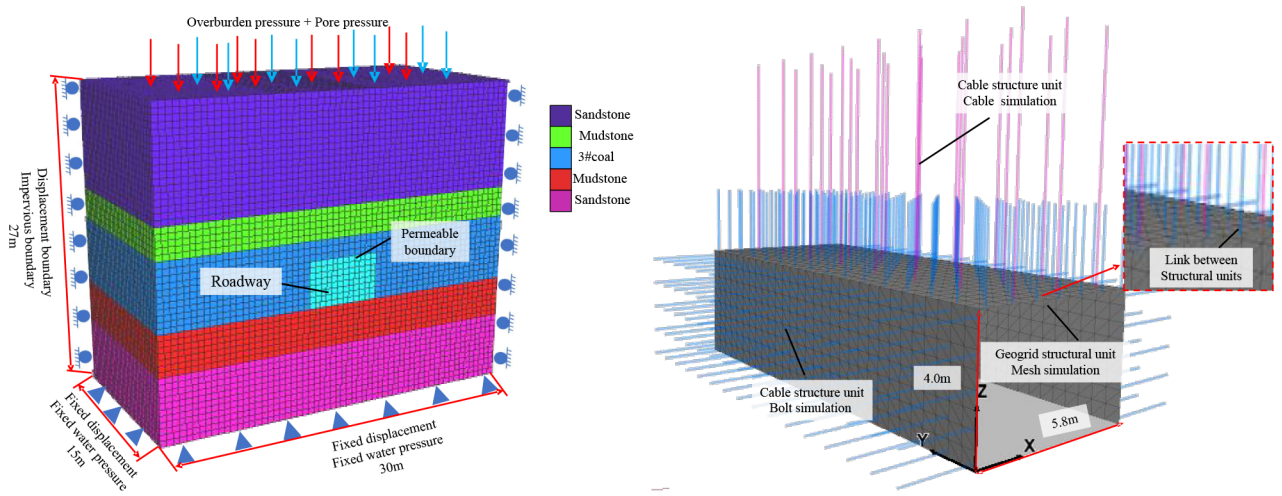

Figure 4. Numerical model and boundary conditions of surrounding rock support in the 2606 roadway.

Table 1. Mechanical Parameters of Coal and Rock Mass in 2606 Transport Roadway of Zhangcun Coal Mine

Rock formation	Density/ g·cm^{-3}	Bulk modulus/ GPa	Shear modulus/ GPa	Cohesion/ MPa	Internal friction angle/deg	Tensile strength/ MPa	Permeability coefficient/m·s^{-1}	Porosity/%
sandstone	2.6	1.84	0.80	2.3	35	2.0	4×10^{-11}	0.6
mudstone	2.5	1.79	0.97	1.9	30	1.6	1×10^{-11}	0.4
coal	1.4	1.66	0.85	1.45	28	1.8	8×10^{-11}	0.5
mudstone	2.6	1.84	0.80	2.3	30	2.0	2×10^{-10}	0.4
sandstone	2.5	1.79	0.97	1.9	38	1.6	1×10^{-10}	0.7

$$p_b = \frac{Q_b}{D_1 D_2} \tag{9}$$

where Q_b is the anchor force of anchor rod, KN; D_1 is the distance between bolts, m; D_2 is the bolt row distance, m.

The cable support resistance is P_c as follows:

$$p_c = \frac{Q_c}{D_1' D_2'} \tag{10}$$

where Q_c is the anchorage force of the cable, KN. D_1' is the cable spacing, m. D_2' is the cable row distance, m.

The metal mesh support resistance for P_{sr} is as follows:

$$p_{sr} = \frac{2\tau_{sr} S_{sr}}{2r \cos\left(\frac{\pi - 2\varphi_1^*}{4}\right)\beta_{sr}} \tag{11}$$

where τ_{sr} is the shear strength of metal mesh material, MPa; S_{sr} is the cross-sectional area of the metal mesh in the axial direction, m^2; β_{sr} is the shear angle of the metal mesh, (deg).

The relationship between the two support methods and the radius of plastic zone is obtained according to eqs 8 to 11, as shown in Figure 3b. In Figure 3b, when the surrounding rock is in the drenching environment, the double-arch joint support method is more effective in controlling the plastic zone of the surrounding rock, thus controlling the stability of the surrounding rock. The high prestressed bolt increases the support strength of the surrounding rock and forms a pressure arch with the mesh. Thereby, the stability of shallow surrounding rock is improved, and the unstable layer of surrounding rock is controlled. As mining time progresses, the number of fissures in the shallow pressure arch will continue to increase, resulting in a gradual decrease in the effective compressive stress formed. The high prestressed cable fully invokes the self-bearing capacity of the deep surrounding rock. The cable and the deep surrounding rock form a pressure arch support system with a more extensive influence range and more robust bearing capacity. The support structure is reasonably matched from time and space to ensure the effective compressive stress superimposed in the deep and shallow surrounding rock pressure arch. The double arches carry the surrounding rock load together to achieve cooperative zoning control and ensure the stability of the surrounding rock.

4. NUMERICAL SIMULATION AND SUPPORT SCHEME DESIGN

4.1. Mechanical Model and Structural Unit Settings.

Based on the engineering geological background of the 2606 transport roadway in the Zhangcun coal mine, a 3D model with a size of 30 m × 15 m × 27 m (length × width × height) is constructed. The roadway in the model is excavated along the bottom floor of the No 3 coal seam, and the roadway section is rectangular with a section size of 5.8 m × 4 m (width × height). To simulate the seepage in the actual project, the top of the 3D model is selected as the permeable boundary, the bottom and the surrounding area are selected as the impermeable boundary, and the roof of the roadway is set as the permeable boundary to simulate the roof seepage. The mechanical boundary conditions are set as follows: The surrounding and bottom surfaces of the model are set as displacement constraints. The upper boundary is free and subjected to the uniform load acting on this boundary by the overlying rock, as shown in Figure 4a. The Mohr-Coulomb constitutive model which conforms to the Mohr-Coulomb failure criterion is used in this statics simulation. The Moore-Coulomb failure criterion is shown below:[47−49]

https://doi.org/10.1021/acsomega.2c05650
ACS Omega 2022, 7, 46682−46692

Table 2. Numerical Simulation Calculation Parameters of Anchor Rod and Anchor Cable

Structure unit	Elastic Modulus/GPa	Diameter/mm	Poisson's ratio	Grout stiffness/MPa	Grout cohesion/MPa	Density/kg·m^{-3}
Bolt	210	22		0.9	1.0	7800
Cable	300	22		0.9	1.0	7850
Mesh	20		0.25			

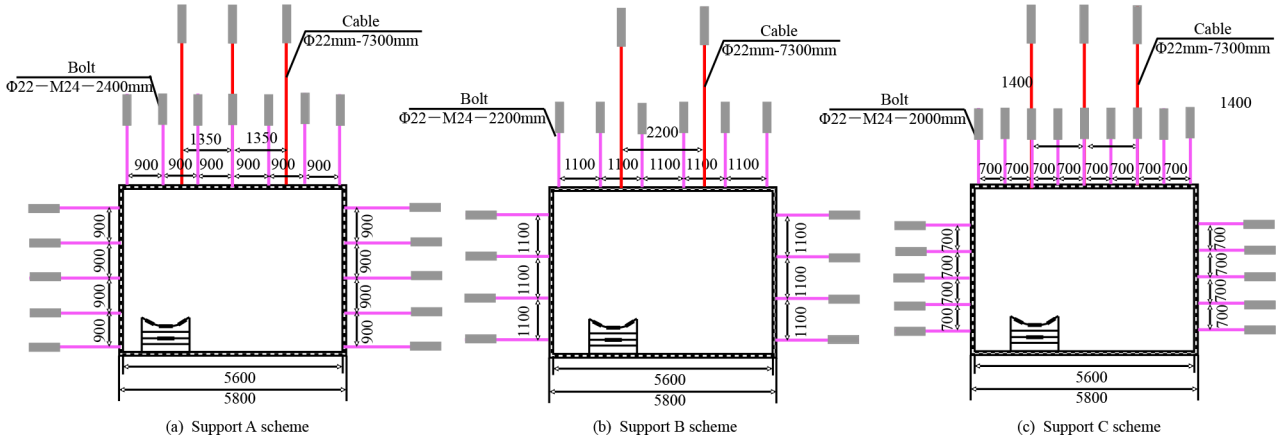

(a) Support A scheme (b) Support B scheme (c) Support C scheme

Figure 5. 2606 roadway support scheme design.

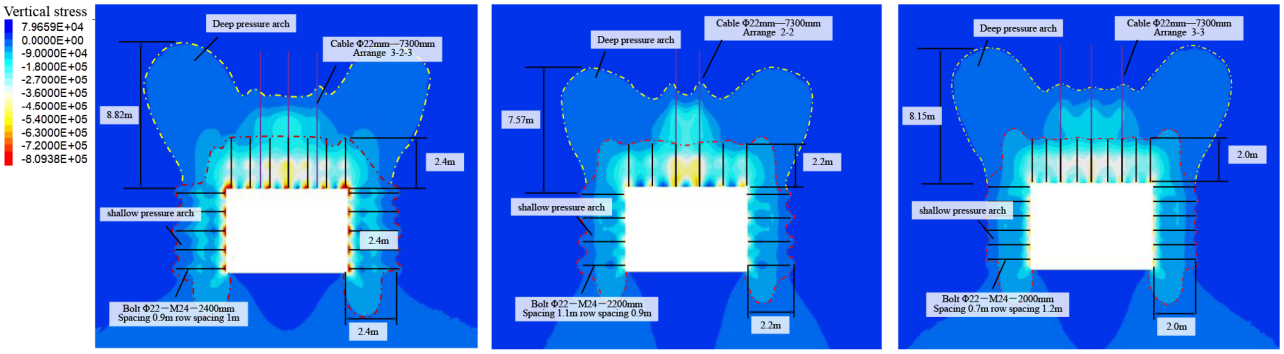

(a) Support A scheme (b) Support B scheme (c) Support C scheme

Figure 6. Evolution law of support stress field in 2606 roadway.

$$f^s = \sigma_1 - \sigma_3 N_\phi + 2C\sqrt{N_\phi} \quad (12)$$

where σ_1 is the maximum principal stress; σ_3 is the minimum principal stress; c is material cohesion; and ϕ is the friction angle;

The coal and rock mechanical parameters used in the numerical simulations cover the literature,[50] as shown in Table 1. The bolt and cable support structure is simulated by the cable structural element of FLAC^{3D} software, and the flexible support of the mesh is simulated by the geogrid structure element.[51,52] Combined with the literature,[53] the parameters of the support structure are shown in Table 2. First, the connection between the bolt, the cable structural element, and the solid element is deleted. Then, a new connection with the mesh structural element is established, and the new node is rigidly constrained. The mesh structural unit and the solid unit are automatically connected to realize the coordinated support of double arch partitions, as shown in Figure 4b.

4.2. Analysis of the Control Effect of Different Support Schemes on Surrounding Rock. According to the principle of "high prestressed bolt, cable + mesh", three support schemes are proposed for simulation and comparison through FLAC^{3D} numerical simulation software. Scheme A is bolt model Φ22-M24−2400 mm (spacing 0.9 m, row spacing 1 m), cable model Φ22 mm-7300 mm (3−2−3); Scheme B is bolt model Φ22-M24−2200 mm (spacing 1.1 m, row spacing 0.9 m), cable model Φ22 mm-7300 mm (2−2); Scheme C is bolt model Φ22-M24−2000 mm (spacing 0.7 m, row spacing 1.2 m), cable model Φ22 mm-7300 mm (3−3), as shown in Figure 5.

4.3. Results and Discussion. *4.3.1. Evolution of Support Stress Field.* Figure 6 shows the evolution law of the support stress field of the 2606 roadway under different support schemes. In Figure 6a, the bolt and the shallow surrounding rock form a shallow pressure arch with a maximum bearing range of 2.4 m, and the cable and the deep surrounding rock form a deep pressure arch, with a maximum influence range of 8.82 m. In Figure 6b, when the distance between the bolts increases from 0.9 m to 1.1 m, there is an anchor void between the bolts. Tensile stress occurs in the anchorage area, resulting in tensile failure of the surrounding rock. When the bolt length is reduced to 2.2 m, the influence range of the shallow pressure arch is reduced by 8.3%. In Figure 6c, when the bolt spacing is reduced from 0.9 m to 0.7 m, the effective compressive stress penetration area between the bolts increases, and there is no anchor void area. However, compared with Scheme A, the

https://doi.org/10.1021/acsomega.2c05650
ACS Omega 2022, 7, 46682−46692

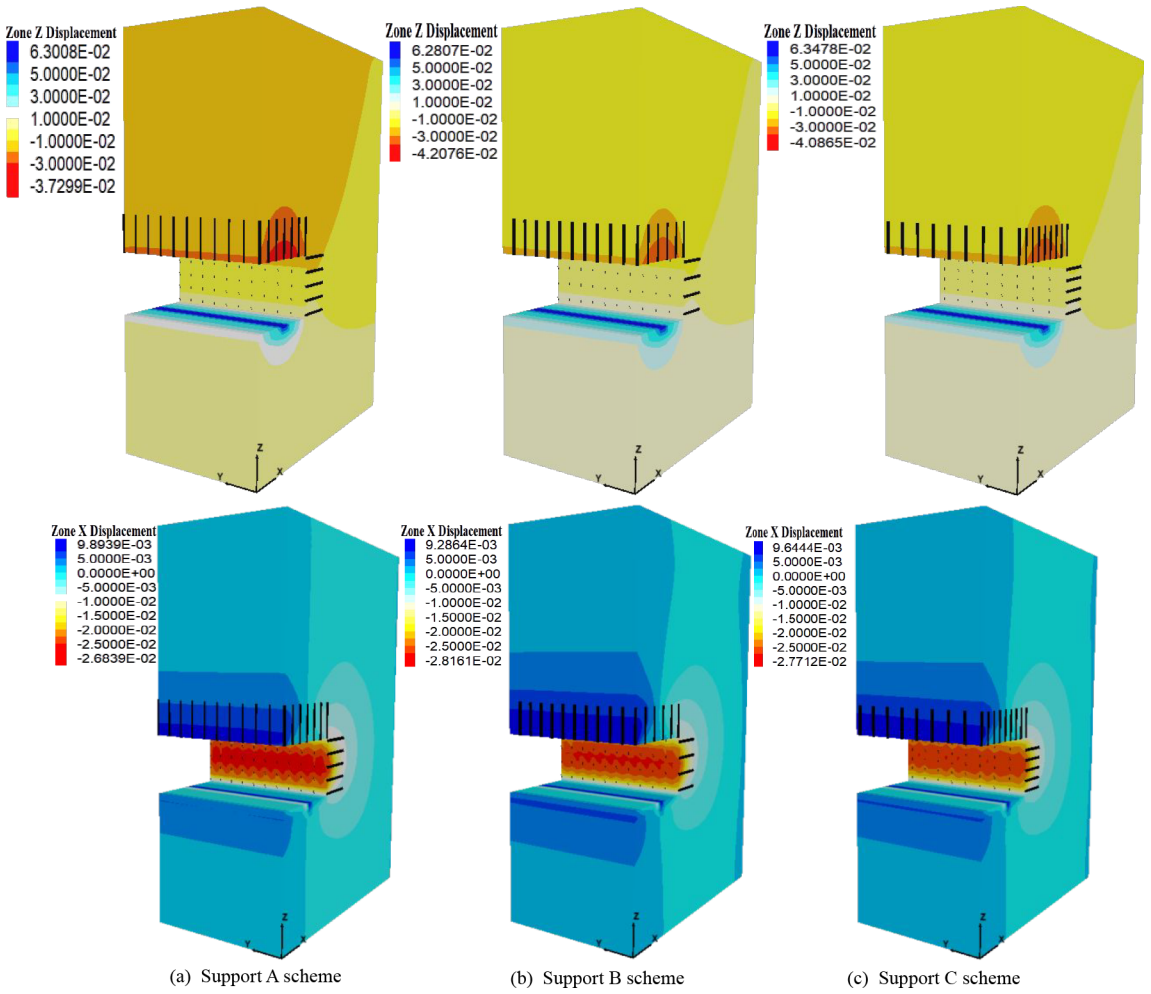

Figure 7. Evolution law of displacement field of surrounding rock in 2606 roadway.

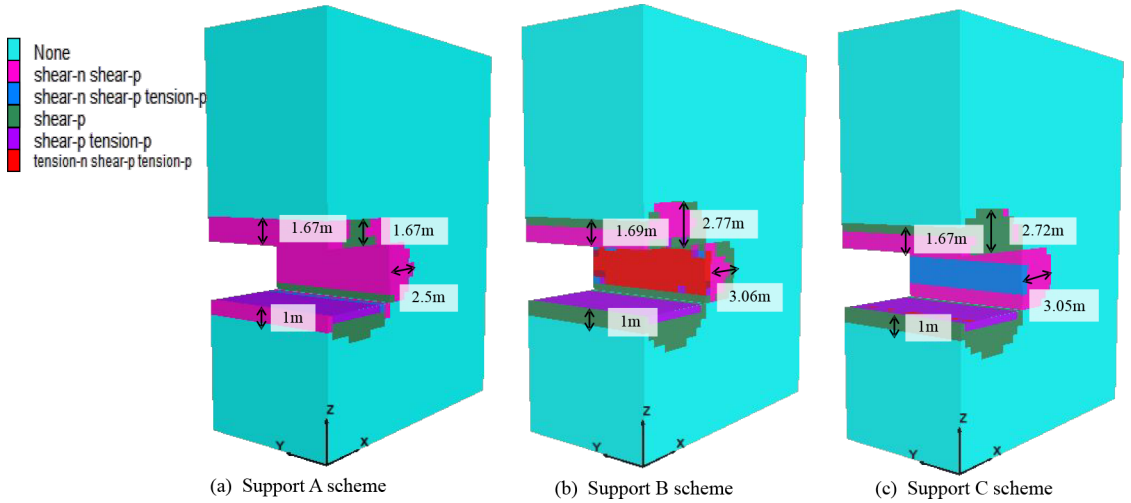

Figure 8. Evolution law of surrounding rock plastic zone of 2606 roadway.

bearing range of the shallow pressure arch is reduced by 16%, and the bearing range of the deep pressure arch is reduced by 7.6%. To sum up, the length and arrangement of the support structure will affect the bearing range of the pressure arch, of which the length is the most important. When scheme A is adopted, the bearing range of the pressure arch formed by the support structure and the surrounding rock is the largest, and there is no anchorage space between the support structures, so scheme A is the optimal support scheme.

4.3.2. Evolution of Displacement Field. Figure 7 shows the evolution law of the surrounding rock displacement field. To observe the change in the excavating direction of the roadway, the model is sliced. From Figure 7a, when scheme A is used for support, the maximum value of the roof subsidence reaches 37

https://doi.org/10.1021/acsomega.2c05650
ACS Omega 2022, 7, 46682−46692

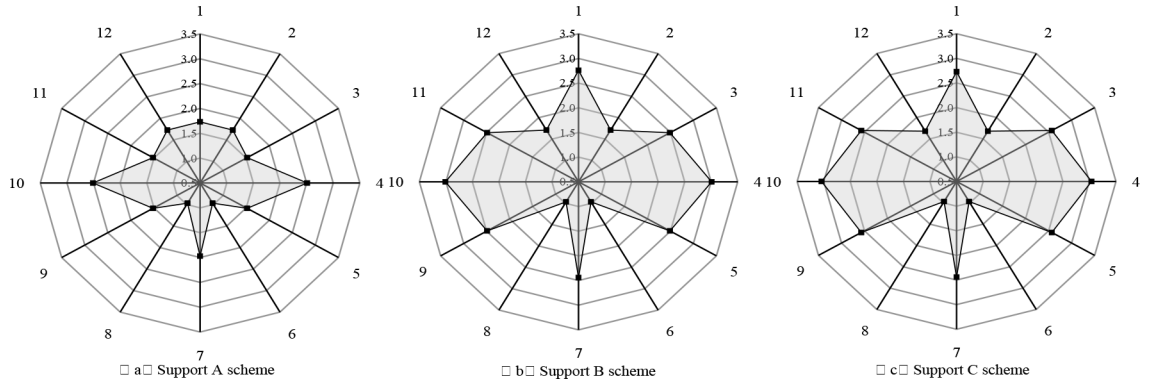

Figure 9. Distribution law of damage range in the plastic zone of 2606 roadway.

mm, and the maximum displacement of the two sides reaches 26 mm. From Figure 7b, when scheme B is used for support, the subsidence of the surrounding rock roof is controlled at 42 mm, and the deformation of the two sides is controlled at 28 mm. Compared with scheme A, the subsidence of the roof is increased by 13.5%, and the deformation of the two sides is increased by 7.14%. From Figure 7c, when scheme C is used for support, the maximum subsidence of the roof is 40.8 mm, and the maximum deformation of the two sides is 27.7 mm. Compared with scheme A, the subsidence of the roof is increased by 9.3%, and the deformation of the two sides is increased by 6.13%.

4.3.3. Evolution of surrounding rock plastic zone. Figure 8 illustrates the evolution law of the plastic zone of surrounding rock under three support schemes. The FISH language was used to extract the volume value of the surrounding rock plastic zone under the three support schemes. In Figure 8a, the support A scheme is adopted. At this time, the tensile failure volume value is 39.26 m^3, and the shear failure volume value is 710.19 m^3. In Figure 8b, the support B scheme is adopted, the roof of the surrounding rock has a tensile failure, and the volume of tensile failure is 78.69 m^3, an increase of 50.1% compared with Figure 8a. The volume value of shear failure of surrounding rock is 753.77 m^3, which is increased by 5.78% compared with Figure 8a. In Figure 8c, the support c scheme is adopted, and the volume value of the surrounding rock with tensile failure is 45.01 m^3, which is 12.77% higher than that in Figure 8a. The volume value of shear failure of the surrounding rock is 760.5 m^3, an increase of 6.61% compared with Figure 8a.

Figure 9 illustrates that 12 azimuth lines were arranged around the surrounding rock to monitor the plastic zone, and the distribution of the maximum and minimum damage range of the plastic zone was obtained. In Figure 9a, when the support A scheme is adopted, the maximum damage range of the roof is 1.67 m, and the maximum damage range of the two sides is 2.5 m. In Figure 9b, when the support scheme B is applied, the damage range of the roof is 2.76 m, an increase of 37.3% compared with the A scheme, and the damage range of the two sides is 3.01 m, an increase of 19.9% compared with the A scheme. In Figure 9c, when the support C scheme is applied, the damage range of the roof is 2.73 m, an increase of 36.6% compared with the A scheme, and the damage range of the two sides is 2.72 m, an increase of 7.72% compared with the A scheme.

5. ENGINEERING PRACTICE

5.1. Engineering Background. Zhangcun Coal Mine is affiliated with Shanxi Lu'an Environmental Protection Energy Development Co., Ltd., located in Changzhi City, Shanxi Province. The buried depth of the coal seam is about 537 m, the thickness of the coal seam is 5.33 m−6.19 m, and the average thickness is 5.86 m. During the excavation of the 2606 roadway, the primitive gas content is 8.5−10.0 m^3/t, and the temperature is 15 °C ∼ 17 °C. 2606 Transport roadway is located on the north side of the 26 belt roadway. The east direction of the 2606 transport roadway is 300 m away from the 2605 transport roadway, as shown in Figure 10. The 2606

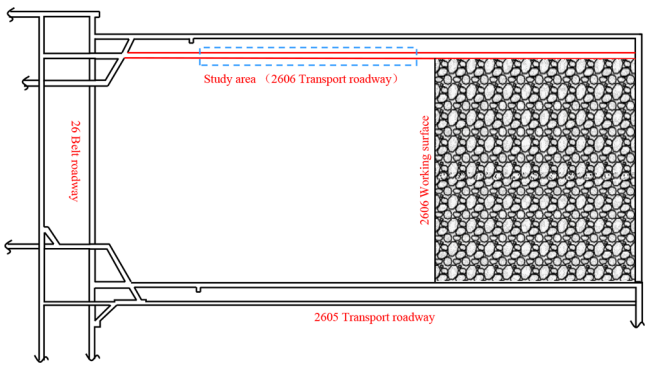

Figure 10. Location of 2606 transport roadway in Zhangcun coal mine

roadway excavation design is arranged along the coal seam floor, leaving 1.5−2 m thick top coal. The immediate roof of the No 3 coal seam is mudstone with a thickness of 2.49 m. The old roof is located in the upper part of the immediate roof. The lithology is medium and fine-grained sandstone, about 7.83 m thick. The immediate floor is mudstone with a thickness of 2.83 m, and the old floor is gray-white fine-grained sandstone with a 5.04 m.

5.2. Deformation Monitoring of Roadway Surrounding Rock. The support scheme of A is applied to the site, the bolt type is Φ22 mm−2400 mm, and the arrangement is 0.9 m spacing and 1 m row spacing; The type of cable is Φ22 mm—7300 mm, and the arrangement is 3−2−3; The mesh is supported by the warp and weft mesh, as shown in Figure 11a. The above support scheme is applied to the 2606 roadway of Zhangcun Coal Mine, and the on-site construction layout is shown in Figure 11b.

https://doi.org/10.1021/acsomega.2c05650
ACS Omega 2022, 7, 46682−46692

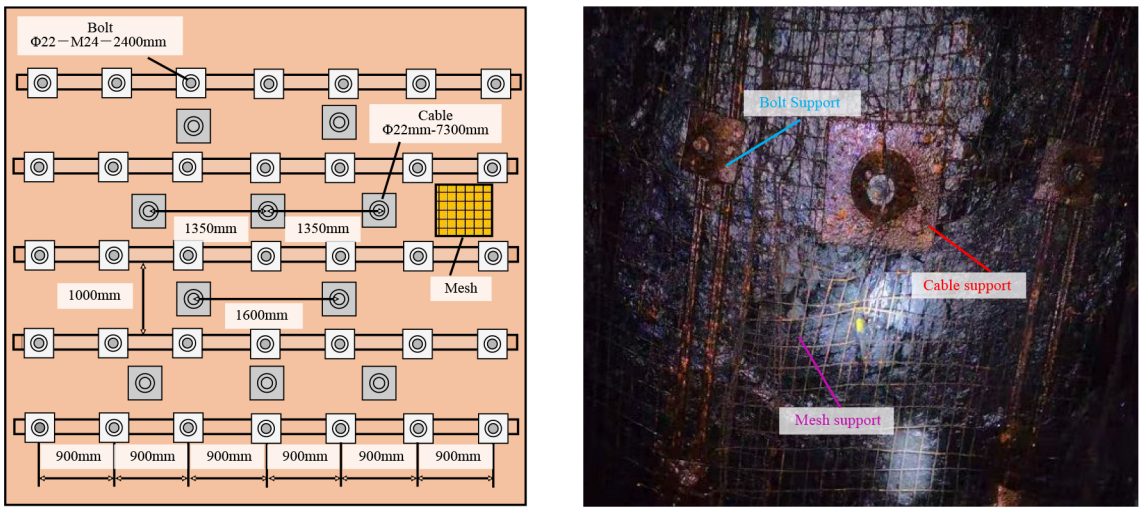

Figure 11. Effect drawing of on-site support of 2606 transport roadway

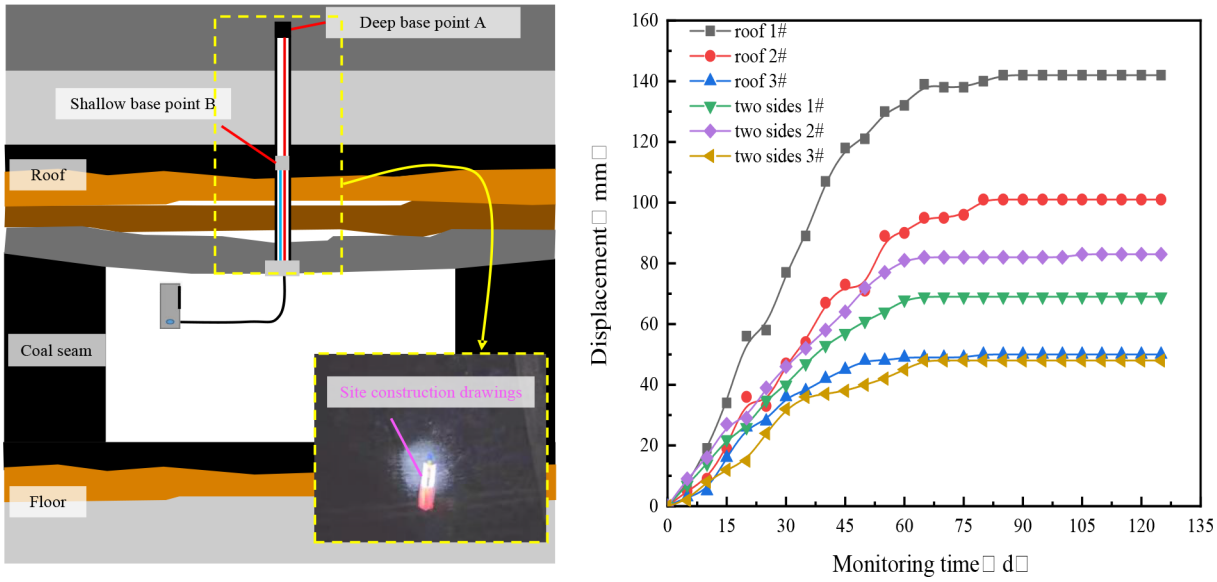

Figure 12. Displacement monitoring of surrounding rock in the 2606 roadway.

The roof separation monitor was installed in the study area, and three monitoring points were arranged. By monitoring the deep displacement of the roadway surrounding rock, the stability of the surrounding rock is judged to evaluate the support scheme.[54] The roof separation monitor adopts a two-point roof displacement measuring instrument, and the 1#−3# monitoring section is equipped with roof separation monitoring. In Figure 12a, points A and B of the roof separation instrument are installed at a depth of 6 m, 2 m.[55] The cross-point method monitors the cross-section surface displacement, and the time-dependent curve of the surface displacement of the 1#−3# section is obtained, as shown in Figure 12b. The deformation of monitoring points 1#−3# is as follows: the deformation of the roof and the two sides increase faster in the first 30d, and the deformation speed gradually slows down around 30d and finally tends to be stable. The maximum deformation of the roof is 142 mm, and the maximum deformation of the two sides is 83 mm. The surrounding rock is effectively controlled.

6. CONCLUSION

(1) In consideration of the effect of water softening on the mechanical damage of surrounding rock, a water-mechanical-damage coupling mathematical model is established. Based on the FLAC^{3D} three-dimensional fast Lagrangian numerical simulation method, the FISH language is used for secondary development to realize the numerical solution of the hydraulic-mechanical-damage coupled mathematical model. There are certain constraints in the model. Nonhomogeneous conditions are not considered and will be added in future investigations.

(2) The principle of "high prestressed bolt, cable + mesh" double-arch zoning cooperative control is revealed. The high prestressed bolt increases the support strength of the surrounding rock and forms a pressure arch with the mesh. Thereby the stability of shallow surrounding rock is improved. The cable and the deep surrounding rock form a pressure arch support system with a more extensive influence range and more robust bearing capacity. Ultimately, the surrounding rock is realized as the double-arch zoning cooperative control.

https://doi.org/10.1021/acsomega.2c05650
ACS Omega 2022, 7, 46682−46692

(3) The three support schemes were compared and analyzed by numerical simulation software. We affirmed the bolt length of 2400 mm, spacing of 0.9 m, row spacing of 1 m, cable length of 7300 mm, and arrangement 3−2−3 as the optimal support scheme and applied the scheme in the Zhangcun Coal Mine. The results show that the subsidence of the roadway roof is 142 mm, and the ultimate convergence of the two sides is 83 mm. The water-drenching roadway has been effectively controlled.

AUTHOR INFORMATION

Corresponding Author

Sheng Li − *College of Mining, Liaoning Technical University, Fuxin 123000, China;* orcid.org/0000-0003-0157-9977; Email: 13941811946@139.com

Authors

Ce Jia − *College of Mining, Liaoning Technical University, Fuxin 123000, China;* orcid.org/0000-0002-3295-0321

Chaojun Fan − *College of Mining, Liaoning Technical University, Fuxin 123000, China;* orcid.org/0000-0003-4578-0760

Mingkun Luo − *Zhangcun Coal Mine, Shanxi Lu'an Chemical (Group) Co., Ltd., Changzhi 046299, China; College of Safety Science and Engineering, Liaoning Technical University, Huludao 125105, China*

Lijun Zhou − *College of Safety Science and Engineering, Liaoning Technical University, Huludao 125105, China*

Ziang Pu − *College of Mining, Liaoning Technical University, Fuxin 123000, China*

Lei Yang − *College of Mining, Liaoning Technical University, Fuxin 123000, China*

Complete contact information is available at: https://pubs.acs.org/10.1021/acsomega.2c05650

Notes

The authors declare no competing financial interest.

ACKNOWLEDGMENTS

The author(s) would like to thank all editors and anonymous reviewers for their comments and suggestions. This research was financially supported by the National Natural Science Foundation of China (Grant Nos. 52174117,52074146 and 51874159), the Natural Science Foundation of Liaoning Province (Grant No. 2020-KF-13-05), Project supported by the Postdoctoral Science Foundation of China (Grant Nos. 2021T140290), and discipline innovation team of Liaoning Technical University (Grant No. LNTU20TD-03).

REFERENCES

(1) Kang, H. P. The 60-year development and prospect of bolt support technology in my country's coal mine roadway. *J.China Univ.Min.Technol.* **2016**, *45*, 1071−1081.

(2) Xie, H. P.; Lu, J.; Li, C. B.; Li, M. H.; Gao, M. Z. Experimental study on the mechanical and failure behaviors of deep rock subjected to true triaxial stress: A review. *Int. J. Min. Sci. Technol.* **2022**, 2095−2686.

(3) Chen, Y. L.; Meng, Q. B.; Xu, G.; Wu, H. S.; Zhang, G. Bolt-grouting combined support technology in deep soft rock roadway. *Int. J. Min. Sci. Technol.* **2016**, *26*, 777−785.

(4) Zhao, Z. Q.; Ma, N. J.; Liu, H. G.; Feng, J. C. Mechanism and early warning method of roof fall in coal seam roadway. *Journal of Coal Industry* **2018**, *43*, 369−376.

(5) Yu, W. J.; Feng, T.; Wang, W. J.; Wang, P.; Yuan, C.; Guo, G. Y.; Du, S. H. Problems and countermeasures of surrounding rock support for thin coal seam mining roadway under complex conditions in southern China. *J. Coal Sci.* **2015**, *40*, 2370−2379.

(6) Wang, B.; Jiang, F. X.; Zhu, S. T.; Zhang, X. F.; Shang, X. G.; Gu, Y. S.; Wu, Z. Mechanism and prevention of high-intensity mining induced scour in the roof drainage area of deep well working face. *J. Coal Sci.* **2020**, *45*, 3054−3064.

(7) Liu, Y. P.; Xia, C.C.; Wu, F. B.; Xu, C.; Deng, Y. G. Research on combined support technology of long and short bolts for soft rock tunnels with high geostress. *Chin. J. Rock Mech. Eng.* **2020**, *39*, 105−114.

(8) Zhan, Q. J.; Shahani, N. M.; Zheng, X. G.; Xue, Z. H. C.; He, Y. Y. Instability mechanism and coupling support technology of full section strong convergence roadway with a depth of 1350 m. *Eng. Failure Anal.* **2022**, *139*, 106374.

(9) Ma, R.; Li, G. C.; Zhang, N.; Liu, C.; Wei, Y. H.; Zhang, M. Analysis on mechanism and key factors of surrounding rock instability in deeply inclined roadway affected by argillation and water seepage. *Int. J. Min. Sci. Technol.* **2015**, *25*, 465−471.

(10) Zhao, Z. H.; Wang, W. M.; Wang, L. H. Theoretical analysis of a new segmented anchoring style in weakly cemented soft surrounding rock. *Int. J. Min. Sci. Technol.* **2016**, *26*, 401−407.

(11) Jia, C.; Li, S.; Fan, C.; Luo, M.; Yang, Z.; Yang, L.; Pu, Z. Instability and failure characteristics of surrounding rock of water drenching roadway in thick coal seam. *Front Earth Sc-Switz.* **2022**, *10*, 1714.

(12) Wang, T.; Yan, C. Z.; Wang, G.; Zheng, Y. C.; Ke, W. H.; Jiao, Y. Y. Numerical study on the deformation and failure of soft rock roadway induced by humidity diffusion. *Tunn Undergr Sp Tech* **2022**, *126*, 104565.

(13) Deng, H. S.; Fu, H. L.; Shi, Y.; Zhao, Y. Y.; Hou, W. Z. Countermeasures against large deformation of deep-buried soft rock tunnels in areas with high geostress: A case study. *Tunn Undergr Sp Tech* **2022**, *119*, 104238.

(14) Yang, T.H.; Jia, P.; Shi, W.H.; Wang, P.T.; Liu, H.L.; Yu, Q.L. Seepage−stress coupled analysis on anisotropic characteristics of the fractured rock mass around roadway. *Tunn Undergr Sp Tech* **2014**, *43*, 11−19.

(15) Yang, R. S.; Li, Y. L.; Guo, D. M.; Yang, Y. M.; Yao, L.; Li, T. T. Failure mechanism and control technology of water-immersed roadway in high-stress and soft rock in a deep mine. *Int. J. Min. Sci. Technol.* **2017**, *27*, 245−252.

(16) Lu, P.*Study on mechanical properties and reasonable grouting parameters of water-rich soft rock tunnel considering fluid-solid coupling*. Thesis, D. Central South University, 2012.

(17) Meng, C.; Li, X. H.; Yao, Q. L.; Zhou, J. Numerical research on stability control of roofs of water-rich roadway. *Int. J. Min. Sci. Technol.* **2014**, *24*, 409−416.

(18) Kang, H. P. 70 years of development and prospect of surrounding rock control methods for coal mine roadways in my country. *Chin. J. Rock Mech. Eng.* **2021**, *40*, 1−30.

(19) Małkowski, P.; Ostrowski, Ł.; Stasica, J. Modeling of floor heave in underground roadways in dry and waterlogged conditions. *Energies* **2022**, *15*, 4340.

(20) Zhai, W. L.; He, F. L.; Xu, X. H.; Lv, K.; Li, L.; Song, J. Y. Floor heave mechanism in water-rich soft rock roadways and a DS-IBA control approach. *Geomat Nat. Haz Risk* **2022**, *13*, 2107−2123.

(21) Zhu, Q. W.; Li, T. C.; Zhang, H.; Ran, J. L.; Li, H.; Du, Y. T.; Li, W. T. True 3D geomechanical model test for research on rheological deformation and failure characteristics of deep soft rock roadways. *Tunn Undergr Sp Tech* **2022**, *128*, 104653.

(22) Xi, P. Q.; Zhu, D. F.; Huo, Y. M.; Xing, C. N.; Wang, Z. L. Numerical Investigation of the Failure Mechanism and Countermeasures of the Roadway Surrounding Rockmass within Deep Soft Rock. *Int. J. Multiscale Comput. Eng.* **2022**, *20*, 20.

(23) He, M. C.; Yuan, Y.; Wang, X. L.; Wu, Z. Q.; Liu, C.; Jiang, Y. L. Control method and application of large deformation of Mesozoic

https://doi.org/10.1021/acsomega.2c05650
ACS Omega 2022, 7, 46682−46692

composite soft rock in Xinjiang. *Chin. J. Rock Mech. Eng.* **2013**, *32*, 433−441.
(24) Tan, Y. L.; Yu, F. G.; Ma, C. F.; Zhang, G. S.; Zhao, W. Research on the coordinated control method of bolt cable-surrounding rock deformation in weakly cemented soft rock roadway. *Coal Sci. Technol.* **2021**, *49*, 198−207.
(25) Zhang, G. C.; He, F. L. Deformation and failure mechanism and control of surrounding rock in high-stress soft rock roadway in deep well. *Journal of Mining & Safety Engineering* **2015**, *32*, 571−577.
(26) Yang, R. S.; Zhu, Y.; Li, Y. L.; Li, W. Y. The mechanism and control countermeasures of the floor heave of the layered floor of the weakly cemented soft rock roadway. *Journal of Mining Safety Engineering* **2020**, *37*, 443−450.
(27) Cai, J. L.; Tu, M.; Zhang, H. L. Study on deformation and instability mechanism of Jurassic weakly cemented soft rock mining roadway and surrounding rock control method. *Journal of Mining Safety Engineering* **2020**, *37*, 1114−1122.
(28) Li, G. C.; Jang, Z. H.; Lv, C. G.; Huang, C.; Chen, G.; Li, M. Y. Instability mechanism and control technology of soft rock roadway affected by mining and high confined water. *Int. J. Min. Sci. Technol.* **2015**, *25*, 573.
(29) Li, B.; Wang, X. Q.; Liu, Z. J.; Li, T. Study on multi-field catastrophe evolution laws of water inrush from concealed karst cave in roadway excavation: a case of Jiyuan coal mine. *Geomat Nat. Haz Risk* **2021**, *12*, 222−243.
(30) Zhao, Y. L.; Peng, Q. Y.; Wan, W.; Wang, W. J.; Chen, B. Fluid−solid coupling analysis of rock pillar stability for concealed karst cave ahead of a roadway based on catastrophic theory. *Int. J. Min. Sci. Technol.* **2014**, *24*, 737−745.
(31) Chen, Y. M.; Xu, D. P.*FLAC/FLAC3D foundation and engineering examples*; China Water & Power Press: Beijing, 2009; pp 193 − 259. (in Chinese).
(32) Zhou, W. F.; Liao, S. M.; Men, Y. Q. A fluid-solid coupled modeling on water seepage through gasketed joint of segmented tunnels. *Tunn Underg r Sp Tech* **2021**, *114*, 104008.
(33) Liu, C.; Zhang, P. S.; Ou, Y. C.; Yao, D. X.; Tian, Y. T. Analytical stress analysis method of interbedded coal and rock floor over confined water: A study on mining failure depth. *J. Appl. Geophys* **2022**, *204*, 104720.
(34) Wang, Q. Y.*Numerical simulation of failure law of unsaturated loess slope induced by rainfall infiltration based on FLAC3D*. Thesis, D. Shijiazhuang railway university, 2019.
(35) Van Genuchten, M. T. A closed-form equation for predicting the hydraulic conductivity of unsaturated soils. *Soil Sci. Soc. Am. J.* **1980**, *44*, 892−898.
(36) Han, P. H.; Zhang, C.; Wang, W. Failure analysis of coal pillars and gateroads in longwall faces under the mining-water invasion coupling effect. *Eng. Failure Anal.* **2022**, *131*, 105912.
(37) Guo, J.; Teng, T.; Zhu, X.; Wang, Y.; Li, Z.; Tan, Y. Characterization and modeling study on softening and seepage behavior of weakly cemented sandy mudstone after water injection. *Geofluids* **2021**, *2021*, 1.
(38) Liu, C. D.; Cheng, Y.; Jiao, Y. Y.; Zhang, G. H.; Zhang, W. S.; Ou, G. Z.; Tan, F. Experimental study on the effect of water on mechanical properties of swelling mudstone. *Eng. Geol.* **2021**, *295*, 106448.
(39) Xu, J.; Li, G.; Rong, H.; Gomah, M. E.; Sun, C.; Li, J.; Zhang, S. Effect of Moisture on the Macro Failure Characteristics of Weakly Consolidated Mudstone Mesomechanism. *Geofluids.* **2022**, *2022*, 2022.
(40) Li, G. C.; Qi, C. C.; Sun, Y. T.; Tang, X. L.; Hou, B. Q. Experimental study on the softening characteristics of sandstone and mudstone in relation to moisture content. *Shock Vib* **2017**, *2017*, 1.
(41) Vergara, M. R.; Triantafyllidis, T. Influence of water content on the mechanical properties of an argillaceous swelling rock. *Rock Mech Rock Eng.* **2016**, *49*, 2555−2568.
(42) Liu, S. M.; Li, X. L.; Wang, D. K.; Zhang, D. M. Investigations on the mechanism of the microstructural evolution of different coal ranks under liquid nitrogen cold soaking. *Energ Source Part A* **2020**, 1−17.
(43) Liu, C. D.; Cheng, Y.; Jiao, Y. Y.; Zhang, G. H.; Zhang, W. S.; Ou, G. Z.; Tan, F. Experimental study on the effect of water on mechanical properties of swelling mudstone. *Eng. Geol.* **2021**, *295*, 106448.
(44) Zhao, C. X.; Li, Y. M.; Liu, G.; Meng, X. R. Mechanism analysis and control technology of surrounding rock failure in deep soft rock roadway. *Eng. Failure Anal.* **2020**, *115*, 104611.
(45) Pan, S.; Liu, S.; Cao, L.; Guo, J.; Yuan, C. Deformation Failure and Support Test of Surrounding Rock in Deep Arched Roadway with Straight Wall. *Adv. Civ. Eng.* **2021**, *2021*, 1.
(46) Li, Y. M.; Zhao, C. X.; Liu, Z. H.; Meng, X. R.; Peng, R. Layered evolution of surrounding rock bearing layer and strength analysis of "layer-double arch" Bearing structure. *J. Rock Mech. Eng.* **2020**, *39*, 217−227.
(47) Lv, J.; Wan, Z.; Yang, Y.; Wang, J.; Zhang, Y.; Liu, S. Failure characteristics and stability control technology of dynamic pressure roadway affected by the mining activity: A case study. *Eng. Failure Anal.* **2022**, *131*, 105857.
(48) Zhou, X. M.; Wang, S.; Li, X. L.; Meng, J. J.; Li, Z.; Zhang, L. H.; Pu, D. D.; Wang, L. K. Research on theory and technology of floor heave control in semicoal rock roadway: Taking longhu coal mine in Qitaihe mining area as an Example. *Lithosphere-Us.* **2022**, *2022* (11), No. 3810988, DOI: 10.2113/2022/3810988.
(49) Wang, S.; Li, X. L.; Qin, Q. Z. Study on surrounding rock control and support stability of Ultra-large height mining face. *Energies* **2022**, *15* (18), 6811.
(50) Zhu, C.; Yuan, Y.; Wang, W.; Chen, Z. S.; Wang, S. Z.; Zhong, H. W. Research on the "three shells" cooperative support technology of large-section chambers in deep mines. *Int. J. Min. Sci. Technol.* **2021**, *31*, 665−68.
(51) Sun, X. M.; Zhu, M. Q.; Zhang, Y.; Zhao, C. W.; Miao, C. Y.; Zhang, S. K. Highly prestressed NPR cable coupling support technology and its application in the deep roadway. *Eng. Failure Anal.* **2022**, *142*, 106707.
(52) Liu, H.; Zhang, B.; Li, X.; Liu, C.; Wang, C.; Wang, F.; Chen, D. Research on roof damage mechanism and control technology of gob-side entry retaining under close distance gob. *Eng. Fail Anal* **2022**, *138*, 106331.
(53) Yu, K. P.; Ren, F. Y.; Puscasu, R.; Lin, P.; Meng, Q. G. Optimization of combined support in soft-rock roadway. *Tunn Undergr Sp Tech* **2020**, *103*, 103502.
(54) Li, X. L.; Chen, S. J.; Wang, S.; Zhao, M.; Liu, H. Study on in situ stress distribution law of the deep mine taking Linyi Mining area as an example. *Adv. Mater. Sci. Eng.* **2021**, *9* (4), 5594181.
(55) Wang, H. W.; Xue, S.; Jiang, Y. D.; Deng, D. X.; Shi, S. Z.; Zhang, D. Q. Field investigation of a roof fall accident and large roadway deformation under geologically complex conditions in an underground coal mine. *Rock Mech Rock Eng.* **2018**, *51* (6), 1863−1883.

https://doi.org/10.1021/acsomega.2c05650
ACS Omega 2022, 7, 46682−46692